2014 IEEE International Conference on Robotics & Automation (ICRA)
Hong Kong Convention and Exhibition Center
May 31 - June 7, 2014. Hong Kong, China

Three Dimensional Modeling of an MRI Actuated Steerable Catheter System

Taoming Liu and M. Cenk Çavuşoğlu, *Senior Member, IEEE*

***Abstract*— This paper presents the three dimensional kinematic modeling of a novel steerable robotic ablation catheter system. The catheter, embedded with a set of current-carrying micro-coils, is actuated by the magnetic forces generated by the magnetic field of the MRI scanner. This paper develops a 3D model of the MRI actuated steerable catheter system by using finite differences approach. For each finite segment, a quasi-static torque-deflection equilibrium equation is calculated using beam theory. By using the deflection displacements and torsion angles, the kinematic modeling of the catheter system is derived. The proposed models are evaluated by comparing the simulation results of the proposed model with the experimental results of a proof-of-concept prototype.**

I. Introduction

Catheter ablation is a widely recognized interventional procedure for treatment of cardiac arrhythmia [1]. During the procedure, the physician typically inserts a catheter into the femoral vein, and guides it into the right atrium, then penetrates it through the atrial septum into the left atrium, as shown in Fig. 1. The catheter tip reaches the desired area required by operator, such as, the ostia of the pulmonary veins (Fig. 1), and applies radiofrequency energy to build ablation barriers to prevent the spread of the irregular electrical signals. During the past decade, a robotic-assisted catheter ablation has increasingly gained many researchers' interests, due to its premise of stable manipulation of the catheter, precise navigation and dexterous control of the catheter tip, and shorter procedure time.

This paper presents the three dimensional kinematic modeling of a steerable robotic ablation catheter system actuated by a novel actuation method which uses the magnetic field of a magnetic resonance imaging (MRI) scanner. In this actuation method, which was originally proposed by Roberts et al. [2] and also investigated by Gudino et al. [3], the catheter is embedded with a set of current-carrying micro-coils. The catheter is actuated by the magnetic forces generated by the magnetic field of the MRI scanner on these coils, by controlling the amount of current going through the coils. The kinematic configuration of the catheter and the deflection under loads of force and torque are modeled using a finite differences approach. The deformation of each segment in the finite differences model is computed using beam theory under mechanical equilibrium conditions. The direct kinematic model is built by using these models.

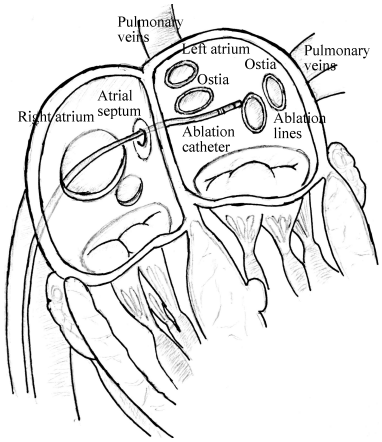

Fig. 1: Illustration of catheter ablation procedure.

The focus of the modeling presented here is the active bending of the catheter to perform the ablation once it is inside the left atrium (Fig. 1). In the ablation procedure, the catheter is remotely controlled by the physician after it is manually inserted into the desired position in the left atrium. Due to the penetration through the atrial septum, which has substantial frictions at this location, it is reasonable to assume that the catheter in the left atrium is fixed to the atrial septum. Our current priority is modeling the catheter's deflection motions in free space and validating this free-space model with the proof-of-concept prototype's experimental results [3], as this modeling will play a significant role in the following research. As the material of the proof-of-concept catheter is the manufacturer's proprietary information, estimating these mechanical parameters based on the experimental results are also presented.

The rest of the paper is organized as follows. Related studies in the literature regarding magnetically steerable catheter systems and catheter modeling are discussed in section II. The modeling of the active catheter is presented in section III. Estimation of the mechanical properties of the catheter prototype is presented in section IV. The validation of the proposed model, including comparisons with experimental deflection results reported in [3], are presented in section V. The discussion and conclusion are presented in section VI.

II. Related Studies

There are several types of active catheters proposed in the literature employing different actuation methods. Magnetic

*This work was supported in part by NSF under grants IIS-0905344 and CNS-1035602, and National Institutes of Health under grants R21 HL096941 and R01 EB018108.

The authors are with the department of Electrical Engineering and Computer Science (EECS) at Case Western Reserve University in Cleveland, OH, USA. The corresponding author M. Cenk Çavuşoğlu can be reached at cavusoglu@case.edu

actuation is one of the active and growing actuation methods employed. One advantage of magnetic actuation is the ability to place the actuation on the tip rather than at the distal end outside patient body, thus increasing the bandwidth by reducing backlash and friction.

In general, there are two ways of using magnetic actuation for catheter's navigation. The first method is to place a permanent magnet on the catheter tip and stay in an external magnetic field. The Niobe® ES magnetic navigation system (Stereotaxis, St. Louis, MO) utilizes two permanent magnets mounted on two pivoting arms located on either side of surgical bed to navigate the catheter [4–6]. The catheter, which has a permanent magnet mounted on its distal tip, is placed in the external magnetic field which can selectively change directions and magnitudes. The attraction and repulsion among the magnets are then used to deflect the catheter as desired. Similarly, Lalande et al. [7] showed that a catheter with some ferromagnetic spheres attached on its tip can be bent and steered inside a MRI system by using magnetic gradients. The second approach is to utilize the physical phenomenon that a current-carrying wire in an external magnetic field is able to produce a magnetic force. Roberts et al. [2], Settecase et al. [8], and Gudino et al. [3], separately demonstrate that a catheter with an array of current-carrying coils mounted on its distal tip can perform an arbitrary 3-dimensional deflection inside clinical MRI scanners. A review of different remote control catheter navigation approaches under MRI is presented in [9].

There are a number of earlier studies on modeling of a catheter under a combined loading. Large deflection models of cantilever beams in a 2-dimensional plane are proposed in the field of mechanics of material [10–12]. Khoshnam et al. [13] modeled the distal section of a catheter by using beam theory. However, these traditional beam theories are not directly extendable to the 3-dimensional catheter deflections as well as torsions. The beam theory can not solve the problem with large deflection angles. Some numerical approaches have been proposed. For example, Cotin et al. [14] assumed the catheter is composed of wire-like segments and developed an incremental finite element model based on beam theory. Lawtwon et al. [15] used rotation group and its algebra to derive the Euler differential equations that described the equilibrium configurations of catheters through potential energy relations. Furthermore, Tunay [6] from Stereotaxis developed a simpler quasi-3D Lawtwon's model.

This paper proposes a new approach combining finite differences approach, beam theory and rotation groups to analyze the catheter's 3D deflection motion. First, the catheter is approximated to be composed of a set of finite segments. The deflection problem of each small segment is assumed to have small deflection angles, and solved by beam theory and the Bernoulli-Euler law. Once each segment's deflection angles and torsion angle are known, the positions of all points on this segment can be found. Considering the each segment as a robot link with the two ends of the segment as the link's joints, the homogeneous transformation relationship between the two ends of the segments are calculated. Using these, the homogeneous transformation relationship between any two ends from two segments can be found. The equilibrium configuration about force and torque of each segment are then set up based on each segment's deflection angles.

III. Methodology

A. Active Catheter Description

The catheter prototype made by mounting an array of current-carrying coils to the tip of a microcatheter, as shown in Fig. 2. The set of coils includes one (or more) axial coil, and two (or more) orthogonal side coils. The catheter is subjected to a combined loading from an array of external magnetic torques on the coils, and the forces from the weights of catheter and steering coils, and lifting force from the fluid.

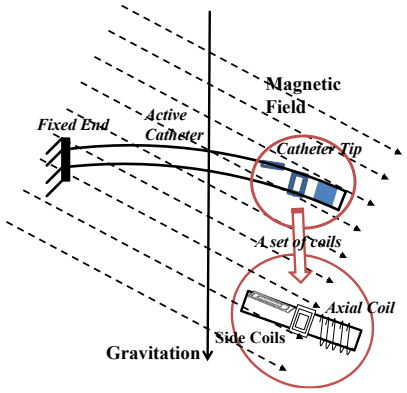

Fig. 2: Illustration of a catheter prototype in a magnetic field, including a set of embedded current-carrying coils.

Several assumptions will be used: 1) Catheter is made of a linear material, that is homogeneous and isotropic.[1] 2) The shear stresses are negligible.[2] 3) Catheter is non-extensible and the strains remain small. 4) The Bernoulli-Euler hypothesis is valid.[3] 5) The bending motion and torsion motion are linearly independent.

B. Modeling of Catheter Deflection Mechanism in Free Space

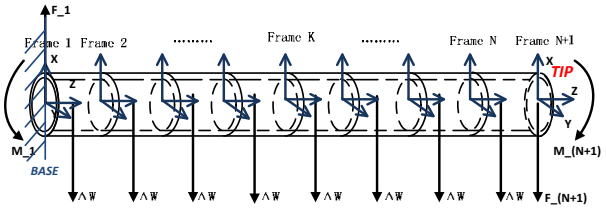

Fig. 3: Diagram of a catheter divided into N finite segments.

[1]Hooke's law is applicable.

[2]The length L of the catheter is much larger than the maximum cross-section diameter D, which indicates the maximum shear stress is small compared to the maximum normal stress. More details are specified in [16].

[3]I.e., plane cross-sections, which are normal to the neutral surface, remain normal during the deformation.

The catheter is a long and tiny tubing. As the deflection angle is sometimes large, this long tubing could not be analyzed as a whole beam by beam theory. Therefore, finite difference approach is applied to analyze the deflection of the catheter by dividing it into N tiny segments (shown in Fig. 3). Each segment has two coordinate frames attached to its two ends. Observed from left to right, the frames are specified as frame 1, frame 2, $\cdots$, frame N, and frame $N+1$. The coordinate frame 1 is catheter's base frame. Here, the rotation matrix R and the rigid body homogeneous transformation g are used to represent the transformation relationship between any two frames. The vector $\overrightarrow{B_1}$ represents the magnetic field relative to the base frame, $[B_x, B_y, B_z]^T$. $\overrightarrow{\mu_1}$, $\overrightarrow{\mu_2}$ and $\overrightarrow{\mu_3}$ represents the magnetization vectors of coil 1, coil 2 and coil 3 relative to frame $N+1$, respectively, where $\overrightarrow{\mu_1}$ = $[1\ 0\ 0]^T$, $\overrightarrow{\mu_2}$ = $[0\ 1\ 0]^T$ and $\overrightarrow{\mu_3}$ = $[0\ 0\ 1]^T$. Hence, the total magnetization vector relative to frame $N+1$ is as follows:

$$\overrightarrow{\mu_{N+1}} = N_1 \mathrm{i}_1 A_1 \overrightarrow{\mu_1} + N_2 \mathrm{i}_2 A_2 \overrightarrow{\mu_2} + N_3 \mathrm{i}_3 A_3 \overrightarrow{\mu_3}, \quad (1)$$

where N_j represents the number of turns in the coil *j*, A_j is the area enclosed by each turn of the coil *j*, and i_j is the current through the coil *j*.

The catheter is also under the load of the gravitational forces and the lifting forces from the blood fluid. In Fig. 3, the total weight F of coils, assumed as a lumped-force, is located at the tip of catheter. The weight of each segment, assumed to be a lumped-force rather than a distributed force, is located in the middle of the segment. The lifting force from the fluid has an opposite direction against gravitational force. So the combined force at each segment is given by

$$\triangle W = (\rho_{cath} - \rho_{fluid}) V h, \quad (2)$$

where V represents the volume of the segment, h is the gravity constant, and ρ_{cath} and ρ_{fluid} represent the density of the catheter and the fluid, respectively.

1) Equilibrium Configurations of the Individual Segments: Fig. 4 shows the free-body diagram of the N^{th} segment, the two ends specified by frame N and frame $N+1$. At the right end, it only has the weight of active coils F_{N+1} relative to the frame $N+1$, and the magnetic torque M_{N+1}. The force F_{N+1} and the torque M_{N+1} can be represented relative to the frame $N+1$,

$$F_{N+1} = R_{N+1,1} F_1, \quad (3)$$
$$M_{N+1} = \hat{\mu}_{N+1}(R_{N+1,1} B_1), \quad (4)$$

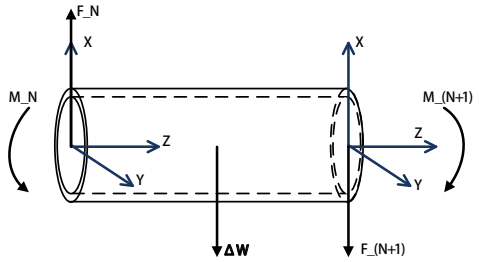

Fig. 4: Equilibrium configurations of the last segment.

where $R_{N+1,1}$ represents the rotation matrix between the frame $N+1$ and the base frame. The equilibrium conditions of the lumped-force $\triangle W$, the torque M_N, and force F_N are

$$F_N = R_{N,1} \triangle W + R_{N,N+1} F_{N+1}, \quad (5)$$
$$M_N = R_{N,N+1} M_{N+1} + P_{N,N+1} \times (R_{N,N+1} F_{N+1}) + Q_{N,N+1} \times (R_{N,1} \triangle W), \quad (6)$$

where $P_{N,N+1}$ represents the vector between the frame N and the frame $N+1$, and $Q_{N,N+1}$ represents the vector between the frame N and the center of this segment.

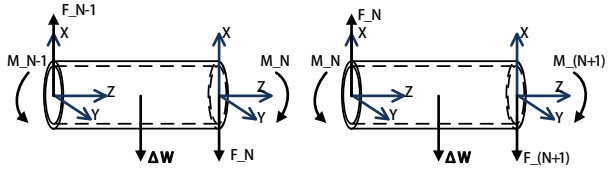

Fig. 5: Equilibrium configurations of two neighbor segments.

The free-body diagrams of the $(N-1)^{th}$ and N^{th} segments are shown in Fig. 5. The equilibrium conditions of the $(N-1)^{th}$ segment are,

$$F_{N-1} = R_{N-1,1} \triangle W + R_{N-1,N} F_N, \quad (7)$$
$$M_{N-1} = R_{N-1,N} M_N + P_{N-1,N} \times (R_{N-1,N} F_N) + Q_{N-1,N} \times (R_{N-1,1} \triangle W). \quad (8)$$

Similarly, for the rest of the segments, the force and torque equilibrium equations can be written for the K^{th} segment, $K \in \{N-2, \cdots, 1\}$, as

$$F_K = R_{K,1} \triangle W + R_{K,K+1} F_{K+1}, \quad (9)$$
$$M_K = R_{K,K+1} M_{K+1} + P_{K,K+1} \times (R_{K,K+1} F_{K+1}) + Q_{K,K+1} \times (R_{K,1} \triangle W). \quad (10)$$

2) Deflection Modeling of the Individual Segments: The deflection of each segment is caused by bending in its X and Y axes, and the torsion around its Z axis.[4] The YZ plane in Fig. 6 (a) shows that this segment is bended by the torque M_x around the positive X axis. The two line segments AB and CD represent the intersection of the YZ plane with the two planes perpendicular to the neutral axis of the segment. The extensions of AB and CD intersect at point O_2, the center of the circularly deformed segment covering an arc of θ_x radians. The radius from the center O_2 to the neutral axis is represented by R. The curve 'ab' is at a distance y from the neutral axis on the positive Y axis. The arc length of the neutral axis is represented by $\triangle s'$.

By the geometry of the sector,

$$\frac{1}{R} = \frac{\theta_x}{\triangle s'}. \quad (11)$$

As the segment has a small deflection, we can approximate

$$\triangle s' \approx \triangle z, \quad (12)$$

[4]These motions obey the assumptions given in Section III-A.

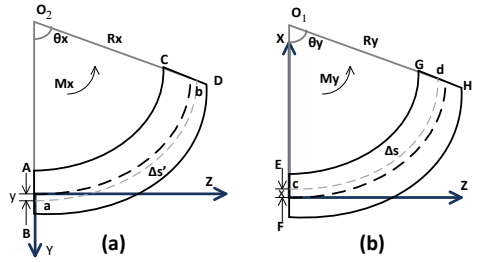

Fig. 6: Diagrams of the deformations of one segment by bending in YZ and XZ planes. (a) Bending in YZ plane. (b) Bending in XZ plane.

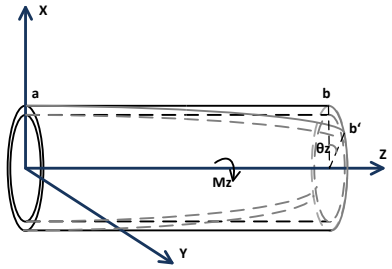

Fig. 7: Diagram of the deformation of one segment by a torsion.

where $\triangle z$ is the length of each segment. So the Eq. 11 is changed to

$$\frac{1}{R} = \frac{\theta_x}{\triangle z}. \tag{13}$$

The geometry of the sector provides the arc length of ab,

$$\widehat{ab} = (R+y)\theta_x = (1+\frac{y}{R})R\theta_x. \tag{14}$$

The strain of this segment equals

$$\epsilon_y = \frac{\widehat{ab} - \triangle z}{\triangle z} = \frac{y}{R}, \tag{15}$$

using Eqs. 13 and 14. Then Eqs. 13 and 15 yield

$$\frac{\epsilon_y}{y} = \frac{1}{R} = \frac{\theta_x}{\triangle z}. \tag{16}$$

As Hooke's law provides the stress-strain relation,

$$\epsilon_y = \frac{\sigma_y}{E}, \tag{17}$$

we obtain

$$\frac{\sigma_y}{Ey} = \frac{\theta_x}{\triangle z}. \tag{18}$$

Applying a similar derivation, the deflection in the XZ plane shown in Fig. 6 (b), can be calculated as

$$\frac{\sigma_x}{Ex} = -\frac{\theta_y}{\triangle z}. \tag{19}$$

Therefore, the normal stress can be calculated as

$$\sigma_z = -\frac{M_x I_{xy} + M_y I_x}{I_x I_y - I_{xy}^2} x + \frac{M_x I_y + M_y I_{xy}}{I_x I_y - I_{xy}^2} y, \tag{20}$$

following an analysis similar to [16], where I_x and I_y are the area moments of inertia of the segment cross section with respect to the X and Y axes, respectively, and I_{xy} is the area product of inertia of the segment cross section.

Eqs. 18, 19, and 20 with $x = 0$ and $y = 0$, respectively, yield

$$\begin{array}{rcl} \frac{M_x I_y + M_y I_{xy}}{E(I_x I_y - I_{xy}^2)} & = & \frac{\theta_x}{\triangle z} \\ -\frac{M_x I_{xy} + M_y I_x}{E(I_x I_y - I_{xy}^2)} & = & -\frac{\theta_y}{\triangle z}, \end{array} \tag{21}$$

which gives the bending angles θ_x and θ_y as a function of moments applied M_x and M_y.

The torsion motion of the catheter is shown in Fig. 7. The moment vector M_z is along the Z axis and the torsional angle is denoted by θ_z. The torsion equation as explained in [16], is

$$\frac{M_z}{GJ} = \frac{\theta_z}{\triangle z}, \tag{22}$$

where G is the shear modulus and J is the polar moment of inertia.

Algebraically, Eqs. 21 and 22 can be arranged into a matrix form as

$$S \cdot \mathbf{M} = C \cdot \mathbf{X}, \tag{23}$$

where

$$S = \begin{bmatrix} I_y & I_{xy} & 0 \\ I_{xy} & I_x & 0 \\ 0 & 0 & 1 \end{bmatrix},$$

$$\mathbf{M} = \begin{bmatrix} M_x & M_y & M_z \end{bmatrix}^{\mathrm{T}},$$

$$C = \frac{1}{\triangle z} \begin{bmatrix} E(I_x I_y - I_{xy}^2) & 0 & 0 \\ 0 & E(I_x I_y - I_{xy}^2) & 0 \\ 0 & 0 & GJ \end{bmatrix},$$

and

$$\mathbf{X} = \begin{bmatrix} \theta_x & \theta_y & \theta_z \end{bmatrix}^{\mathrm{T}}.$$

Simultaneous solutions of Eq. 23 for all of the segments would yield the deflection and torsion angles for all segments. Once the deflection angles are calculated, the coordinate of the end point on each segment can be calculated as

$$P = \begin{bmatrix} \frac{\triangle Z(1-\cos(\theta_y))}{\theta_y} \\ -\frac{\triangle Z(1-\cos(\theta_x))}{\theta_x} \\ \frac{1}{2}(\frac{\triangle Z \sin(\theta_x)}{\theta_x} + \frac{\triangle Z \sin(\theta_y)}{\theta_y}) \end{bmatrix} \tag{24}$$

in its own frame.

IV. Estimation of Catheter Prototype's Mechanical Parameters

The quantitative comparisons between the simulation results of the proposed model and the experimental results of the catheter prototype presented in [3] under the same experimental environment validate the proposed model of the catheter system. Fig. 8 shows this proof-of-concept prototype built by Gudino [3], which is made by a 2.5 Fr (0.83mm) fiber braided microcatheter (Renegade, Boston Scientific).

An array of current-carrying coils made of 42 gauge wire is mounted at the tip of the catheter, coil 1 with a 15-turn square side coil, coil 2 with a 70-turn axial coil and coil 3 with a 70-turn axial coil. It is immersed in a water phantom containing 1% Gd-DTPA, which is placed in MRI scanner. The experimental setup is shown in Fig. 9. The

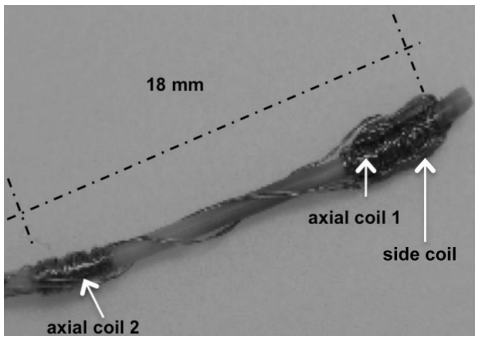

Fig. 8: Diagram of the proof-of-concept catheter prototype [3].

magnetic field with an amplitude of B_1 = 1.5 T, is pointing horizontally right and perpendicular to the catheter shape in zero configuration. The direction of gravity points vertically down. The experimental result of the total deflection of the catheter is shown with black markers in Fig. 10(a). They measure 8 quantitative deflections with 8 different currents by exciting coils.

However, the actual material of this microcatheter is unknown, as it is the proprietary information of the catheter manufacturer. We need to estimate the mechanical parameters of this catheter material, i.e., its density, young's modulus, poisson's ratio and shear's modulus, prior to the validation of the proposed models. Additionally, the experimental data indicates that there is an initial catheter tip deflection, 1.5991 cm as shown in Fig. 10(a), when no current input to the catheter, due to the natural bent of the catheter. In this study, this rest bending of the catheter is approximately

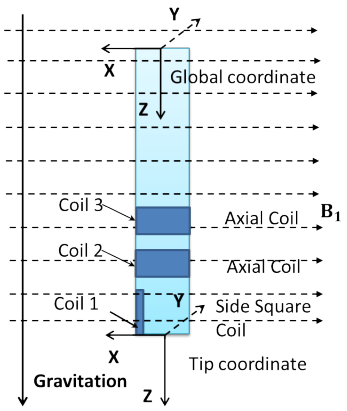

Fig. 9: Simplified diagram of the catheter in a magnetic field. Coil 1 is the square side coil. Coil 2 and 3 are the axial coils. B_1 = 1.5 T. The direction of the magnetic field points right, while the direction of the gravity points down.

modeled by an external force acting on the catheter tip, which also needs to be estimated.

These parameters are estimated from 3 data points, corresponding to the rest deflection of the catheter (no current applied), largest deflection obtained by exciting all three coils at 100 mA, and the deflection obtained by exciting only the distant axial coil at 130 mA. The parameters are then estimated by finding the set of parameters that minimizes the error between the actual deflection measurements and the deflections estimated by the model.

The computation of this minimization problem provides us a set of appropriate parameters as: young's modulus $350MPa$, poisson's ratio 0.3, density $900kg/m^3$, and the external force $2.00 \times 1.0e^{-4}N$.

V. Simulation Results

Equipped with the appropriately estimated mechanical parameters obtained in Section IV, the proposed model is

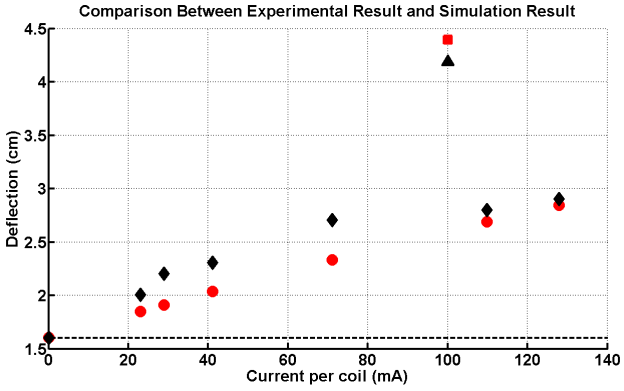

(a)

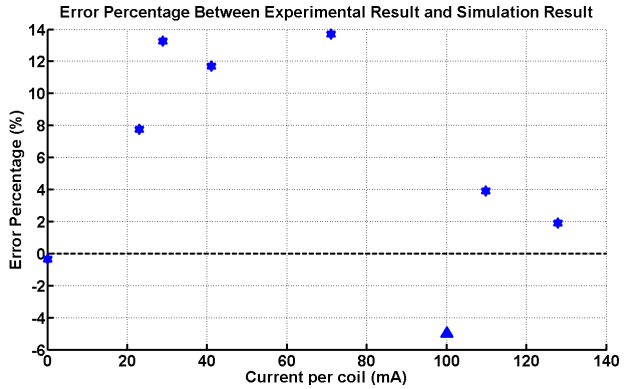

(b)

Fig. 10: The simulation result of the deflection of the catheter by sequentially exciting active coils. (a) The black diamonds represent the experimental deflections by exciting only the distal axial coil and the black triangle represents the largest deflection in the experiment. The red circles represent the simulation deflections by exciting the same axial coil and the red square represents the largest deflection in the simulation. (b) The percentage error between the simulation results and experimental results.

used to estimate the total deflection of the catheter by sequentially exciting the active coils, as shown in Fig. 10. The experimental results obtained by exciting only the distal axial coil at the tip from 0 mA to 130 mA, are marked with black diamonds in Fig 10(a). Under the same excitation, the simulation deflections computed by the proposed model are marked with the red circles. The black triangle represents the largest experimental deflection by exciting all active coils, while the red square represents the corresponding largest deflection in the simulation. Fig. 10(b) shows the percentage error between the corresponding experimental and simulation deflections. It is confirmed that the percentage errors of the three characteristic deflections are small, as minimizing them gets the estimation parameters. The largest percentage error is less than 14%. These comparisons demonstrate that the model matches with the experimental results.

VI. Discussion and Conclusion

In this paper, a 3D model of a steerable catheter using an array of active steering coils in a magnetic field in free space is presented. In the proposed method, the catheter is modeled as a series of finite segments. The deflection displacement and torsion angle for each segment at the quasi-static equilibrium condition were calculated using beam theory. The catheter's deflections estimated by the proposed model matches with the experimental results collected by Gudino et al. [3] under the same experimental conditions.

The computation time of the proposed model for computing the tip location is important concerns for clinical applicability of the methods. The numerical computation of the direct kinematic model given the current inputs takes approximately 4 seconds on a computer equipped with Intel® core i7-960 CPU @ 3.20 GHz and 12.0 GB memory, running 64-bit Microsoft Windows 7 operating system. The calculation is implemented in Matlab® 7.11.0 (R2010b).

In the future, this proposed catheter model will be used to optimize the catheter prototype design according to the clinical ablation application. The design issues include the selection of the material and the dimension of the catheter, the type and the number of coils, the number of winding per each coil, the placement of the coils and so on.

References

[1] *What Is Catheter Ablation?*, National Heart Lung and Blood Institute, http://www.nhlbi.nih.gov/health/health-topics/topics/ablation/.

[2] T. P. Roberts, W. V. Hassenzahl, S. W. Hetts, and R. L. Arenson, "Remote control of catheter tip deflection: an opportunity for interventional MRI," *Magnetic Resonance in Medicine*, vol. 48, no. 6, pp. 1091–1095, December 2002.

[3] N. Gudino, J. A. Heilman, J. J. Derakhshan, J. L. Sunshine, J. L. Duerk, and M. A. Griswold, "Control of intravascular catheters using an array of active steering coils," *Medical Physics*, vol. 38, no. 7, pp. 4215–4224, July 2011.

[4] *Niobe® ES Magnetic Navigation System*, Stereotaxis, http://www.stereotaxis.com/niobe.html.

[5] I. Tunay, "Position control of catheters using magnetic fields," in *Mechatronics, 2004. ICM '04. Proceedings of the IEEE International Conference on*, June 2004, pp. 392–397.

[6] ——, "Modeling magnetic catheters in external fields," in *Proceedings of the 26th Annual International Conference of the IEEE EMBS*, San Francisco, CA, USA, September 1-5, 2004, pp. 2006–2009.

[7] V. Lalande, F. P. Gosselin, and S. Martel, "Catheter steering using a magnetic resonance imaging system," in *32nd Annual International Conference of the IEEE EMBS*, August 31 - September 4 2010.

[8] F. Settecase, M. S. Sussman, M. W. Wilson, S. Hetts, R. L. Arenson, V. Malba, A. F. Bernhardt, W. Kucharczyk, and T. P. L. Roberts, "Magnetically-assisted remote control (MARC) steering of endovascular catheters for interventional MRI: a model for deflection and design implications," *Medical Physics*, vol. 34, no. 8, pp. 3135–3142, August 2007.

[9] L. Muller, M. Saeed, M. Wilson, and S. Hetts, "Remote control catheter navigation: options for guidance under MRI," *Journal of Cardiovascular Magnetic Resonance*, vol. 14, no. 1, p. 33, 2012.

[10] L. Chen, "An integral approach for large deflection cantilever beams," *International Journal of Non-Linear Mechanics*, vol. 45, no. 3, pp. 301 – 305, 2010.

[11] K. Lee, "Large deflections of cantilever beams of non-linear elastic material under a combined loading," *International Journal of Non-Linear Mechanics*, vol. 37, no. 3, pp. 439 – 443, 2002.

[12] T. Belendez, C. Neipp, and A. Belendez, "Large and small deflections of a cantilever beam," *European Journal of Physics*, vol. 23, no. 3, p. 371, 2002.

[13] M. Khoshnam, M. Azizian, and R. V. Patel, "Modeling of a steerable catheter based on beam theory," in *IEEE International Conference on Robotics and Automation*, RiverCenter, Saint Paul, Minnesota, USA, May 14-18 2012.

[14] S. Cotin, C. Duriez, J. Lenoir, P. Neumann, and S. Dawson, "New approaches to catheter navigation for interventional radiology simulation," in *: Proceedings of Medical Image Computing and Computer Assisted Intervention (MICCAI), Palm*, 2005, pp. 300–308.

[15] W. Lawton, R. Raghavan, S. R. Ranjan, and R. Viswanathan, "Ribbons and groups: a thin rod theory for catheters and filaments," *Journal of Physics A: Mathematical and General*, vol. 32, no. 9, p. 1709, 1999.

[16] A. P. Boresi and R. J. Schmidt, *Advanced Mechanics of Materials*, 4th ed. John Wiley and Sons, Inc, 1985.